Supporting Information:

Low-Dosage Viscosity Breakdown and Mechanistic Insights into Cu-MOF-74/PMS Degradation of High-Concentration Polyacrylamide

Qiuxuan Dong[a, b], Yan Shu[a], Yihai Yang[a], Mingxing Bai[c], Peisong Shi[a], Miao Wang[d], Guolin Jing [a]*, Zhengnan Sun [a]*

[a] *Provincial Key Laboratory of Oil and Gas Chemical Technology, College of Chemistry and Chemical Engineering, Northeast Petroleum University, Daqing, Heilongjiang, China, 163318.*

[b] *School of Physics and Electronic Engineering, Northeast Petroleum University, Daqing, 163318, China*

[c] *School of Petroleum Engineering, Northeast Petroleum University, Daqing 163318, China*

[d] No.4 Oil Production Plant of Daqing Oilfield Co., ltd, Daqing 163318, China

E-mail address:

Qiuxuan Dong: msdongqiuxuan@163.com;

Yan Shu: 1642812934@qq.com;

Yihai Yang: yangyh0314@163.com;

Mingxing Bai: bai510714@163.com;

Peisong Shi: ax6386@163.com;

Miao Wang: sin0459@163.com;

Guolin Jing (corresponding author): jglxueshu@yeah.net;

Zhengnan Sun (corresponding author): sunzhengnan@nepu.edu.cn.

Contact address: NO.99 development road of Daqing, People's Republic of China.

Text

S1. Materials

HPAM and SRPAM powder samples were obtained from an oilfield in Daqing, with a molecular weight of 25 million Da. Potassium peroxymonosulfate triple salt ($2KHSO_5 \cdot KHSO_4 \cdot K_2SO_4$), copper(II) nitrate trihydrate ($Cu(NO_3)_2 \cdot 3H_2O$), 2,5-Dihydroxyterephthalic acid (DHTA), gpolyvinyl pyrrolidone (PVP), N.N-Dimethylacetamide(DMAC), hydroxide (NaOH), concentrated sulfuric acid (H_2SO_4), sodium chloride (NaCl), sodium carbonate (Na_2CO_3), sodium bicarbonate ($NaHCO_3$), sodium sulfate (Na_2SO_4), magnesium chloride hexahydrate ($MgCl_2$, $6H_2O$), calcium chloride ($CaCl_2$), methanol (MeOH), L-histidine (L-his), tert-butanol (TBA), p-benzoquinone (p-BQ). Aladdin Reagent Co., Ltd. Shanghai, analytical grade.

S2. Analytical methods

(1) Material characterization

The morphological characteristics, crystalline structure, and functional group composition of the materials were characterized using scanning electron microscopy (SEM, Hitachi S4800, Japan), Transmission electron microscopy (TEM, FEI Tecnai G2 F20, Netherlands), X-ray diffraction (XRD, PANalytical X'pert3, Netherlands), and attenuated total reflection Fourier transform infrared spectroscopy (ATR-FTIR, Bruker Tensor 27, Germany), respectively. Using a thermogravimetric analyzer (TGA, Hitachi TG/DTA7300, Japan), the thermal stability of Cu-MOF-74 was assessed in air by heating from 35 °C to 550 °C at 10 °C/min. Its textural properties, including specific surface area and pore size distribution, were analyzed via N_2 adsorption-desorption(BET, Kantar NOVA2000, USA). All samples were pre-degassed at 150 °C for 6 hours before measurements at 77 K. The concentration of ion release in the solution was determined using inductively coupled plasma optical emission spectrometry (ICP-OES, Agilent 5800, USA). The chemical surface properties of Cu-MOF-74 were characterized by X-ray photoelectron spectroscopy (XPS, Thermo Scientific K-Alpha, USA), while the temporal viscosity change of the HPAM solution during degradation was tracked with a Brinell rotational viscometer (DV-II+Pro, Brookfield, USA). To analyze the reactive radical species, electron Paramagnetic resonance (EPR, Bruker, Germany) spectroscopy was employed with 5,5-dimethyl-1-pyrroline N-oxide (DMPO) and 2,2,6,6-tetramethylpiperidine (TEMP) as spin trapping agents for free radicals and non-radical species, respectively. In addition, the compositional changes of HPAM before and after degradation were determined by UV-Vis spectrophotometer (UV-Vis, Thermo Evolution 220, USA), and evaluating solution stability via zeta potential and particle size measurements on a Zeta potential and nanoparticle size analyzer (Brookhaven ZetaPALS, USA). HPAM degradation intermediates were identified using gas chromatography-mass spectrometry (GC/MS, Thermo Trace 1610/Orbitrap Exploris GC 240, Japan). Chromatographic conditions: TG-5SILMS capillary column (30 m × 0.25 mm × 0.25 μm), helium carrier gas (99.999%) at 1.0 mL/min, inlet temperature 300 °C, split ratio 50:1, and programmed temperature ramp: 40 °C (2 min)→20 °C/min→300 °C (15 min). Mass spectrometry parameters: EI ionization (70 eV), ion source temperature 230 °C, scanning range 30-450 m/z.

(2) Calculation formulas

The viscosity of the water samples was measured using a Brookfield rotational viscometer coupled with a constant-temperature water bath system. An S-01 rotor was used for the measurements at a set rotational speed of 10 r/min. After configuring the instrument, approximately 40 ml of the sample was placed into the measuring container. The viscometer was then started, and data were recorded once the readings stabilized, representing the steady-state viscosity.

The formula for the viscosity reduction rate is shown in equation (1) [1].

$$\Delta\eta = \frac{(\eta_0 - \eta)}{\eta_0} * 100 \quad (1)$$

Where: $\Delta\eta$ is the viscosity reduction rate, %; η_0 is the initial viscosity of HPAM solution, mPa·s; η is the viscosity of HPAM solution after reaction, mPa·s.

Figures and Tables

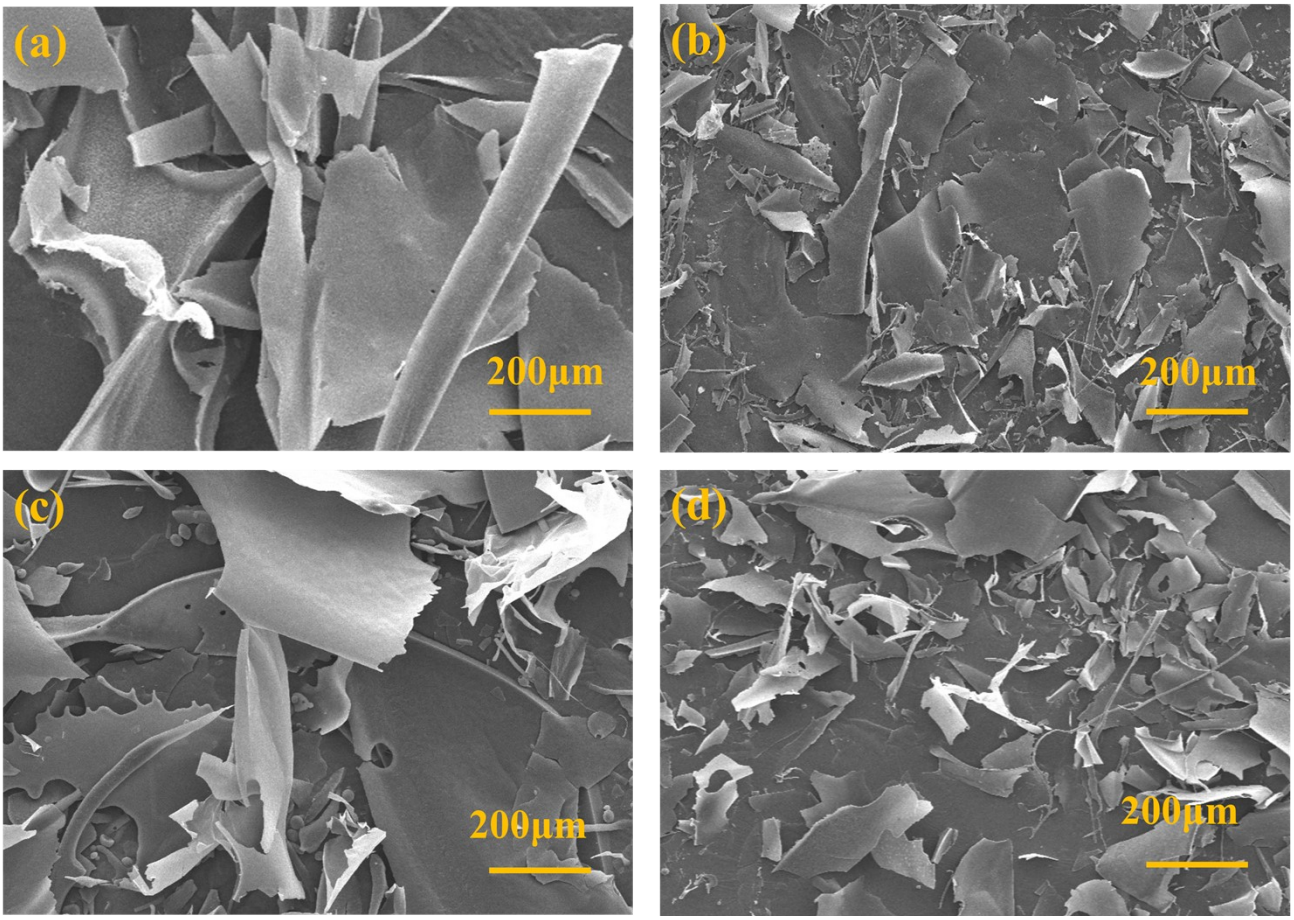

Fig. S1. SEM images of HPAM (a, b) and SRPAM (c, d) before and after the reaction, respectively.

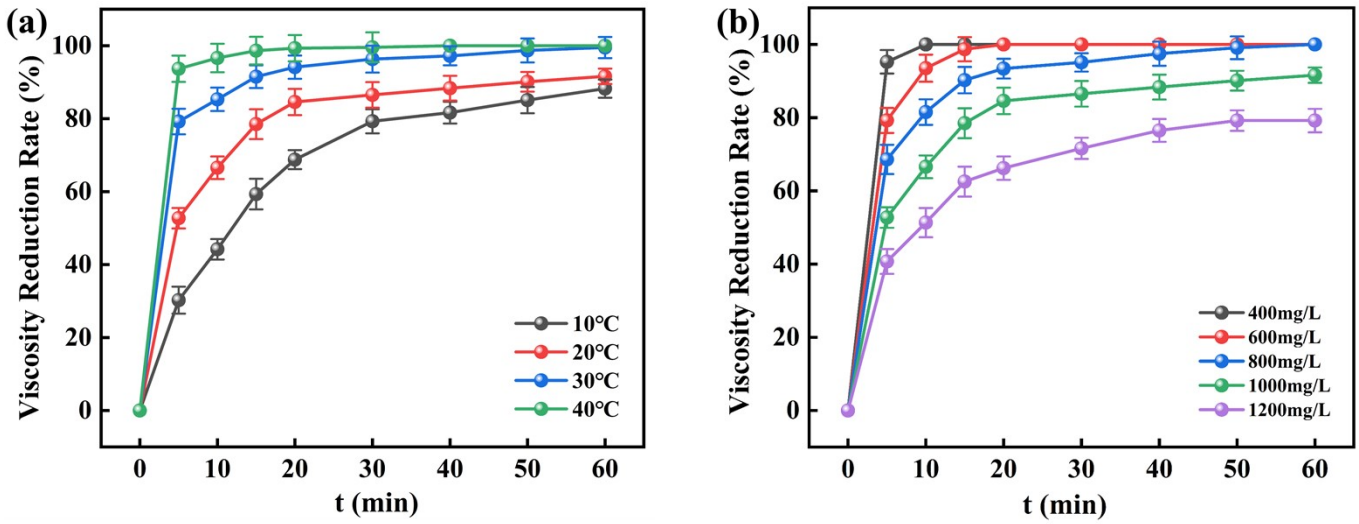

Fig. S2. Effect of different temperatures(a), HPAM concentrations(b) on viscosity reduction of HPAM. Reaction condition: T = 20°C, $[HPAM]_0$ = 1000 mg/L, $[Catalyst]_0$ = 7 mg/L, and $[PMS]_0$ = 0.2 mmol/L.

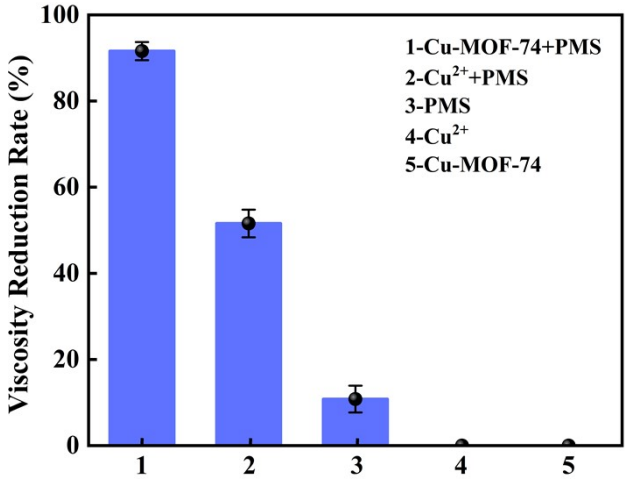

Fig. S3. Control experiments for HPAM viscosity reduction under different conditions. Reaction condition: T = 20℃, $[HPAM]_0$ = 1000 mg/L, $[Catalyst]_0$ = 7 mg/L, $[Cu^{2+}]_0$ = 0.49 mg/L, and $[PMS]_0$ = 0.2 mmol/L.

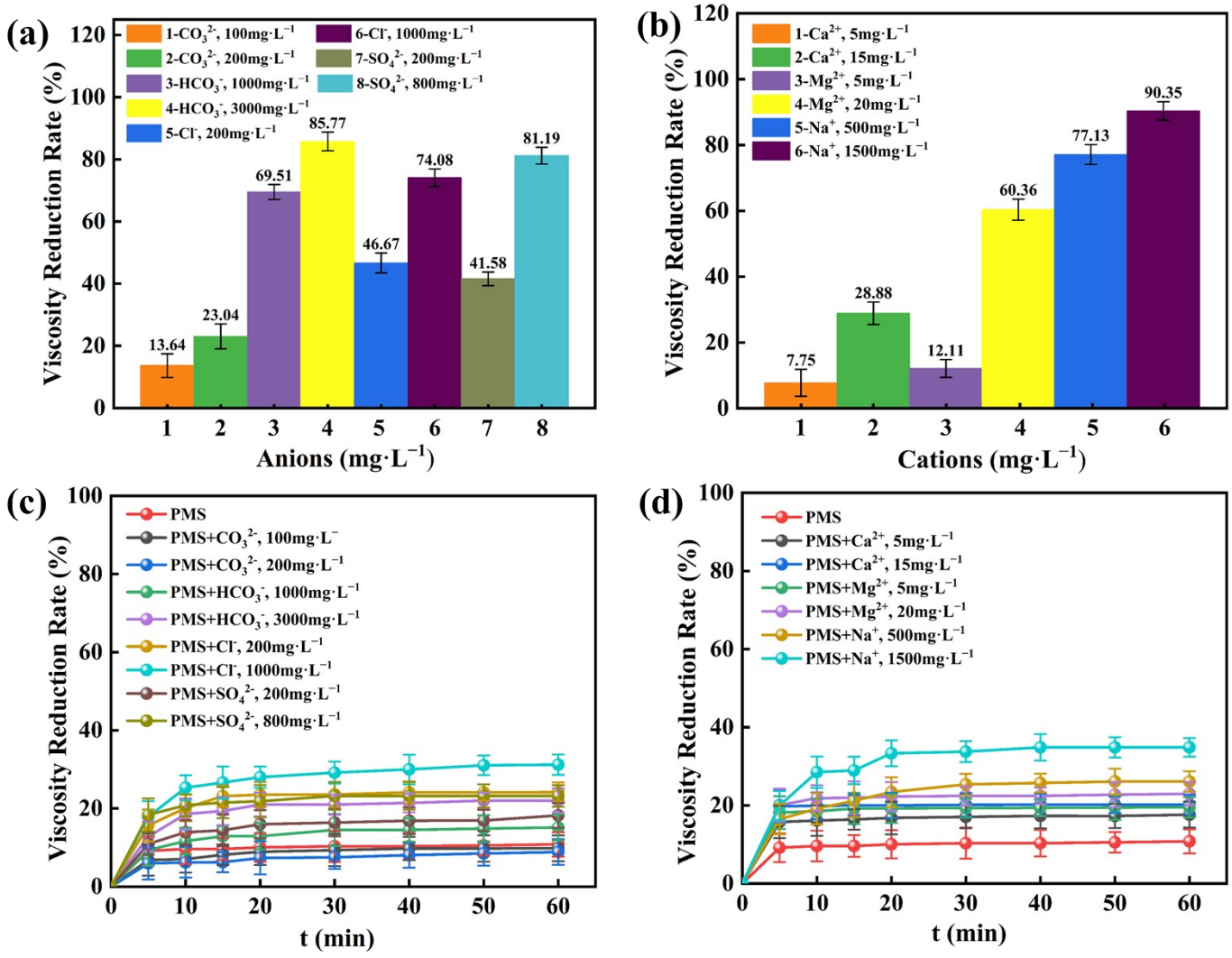

Fig. S4 Effects of ions on HPAM viscosity and PMS oxidation: (a) anions, and (b) cations effects on HPAM viscosity; (c) anions, and (d) cations effects on PMS oxidation. Reaction condition: T = 20℃, $[HPAM]_0$ = 1000 mg/L, and $[PMS]_0$ =

0.2 mmol/L.

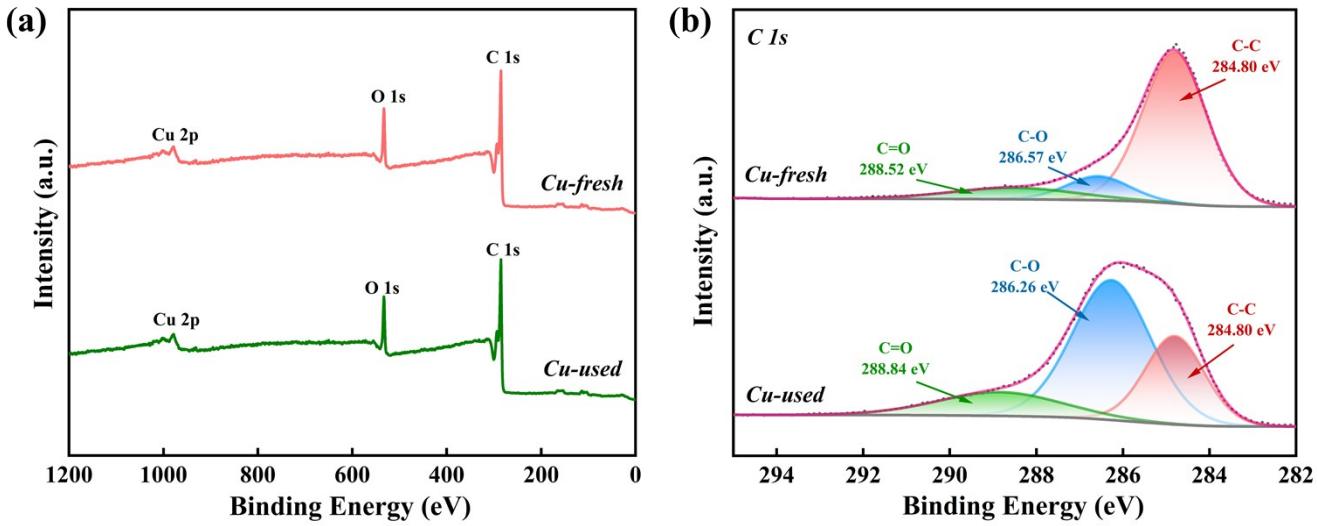

Fig. S5. XPS full survey(a) and C 1s(b) spectra of Cu-MOF-74 before and after reaction.

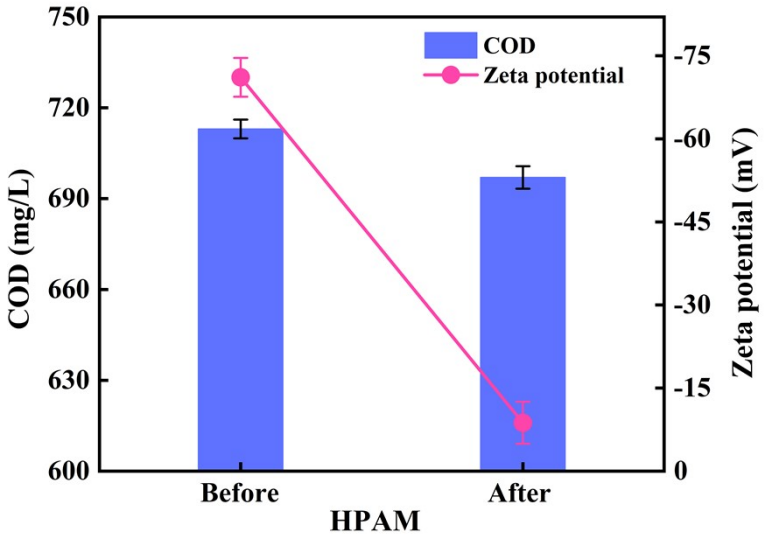

Fig. S6. COD and Zeta potential spectrum.

Table S1. BET data of Cu-MOF-74

Name	Surface area m^2/g	Total pore volume cm^3/g	Average pore diameter nm
Cu-MOF-74	137.333	0.2889	9.52

Table S2. GC/MS of Cu-MOF-74 after reaction

Time/min	Molecular formula	Name	Source
1.11	CH_2O	Formaldehyde	Backbone cleavage and oxidation
3.68	C_3H_6O	Acetone	Side-chain or terminal oxidation
5.41	$C_3H_4\mathbf{O_2}$	Acrylic acid	Acrylamide oxidation
7.45-7.96	C_3H_5NO	Acrylamide	Backbone C–C scission
9.08	C_3H_7NO	Propionamide	Backbone C–C scission
9.89	C_4H_9NO	Butyrylamide	Medium or short fragments
11.52	$C_6H_{13}NO$	Hexanamide	Long fragments

14.32	—	Nitrogen-containing heterocycles or long-chain fatty acid derivatives	Large residues (with amide groups)

References

1. B. Zhu, G. Jiang, Y. Lv, F. Liu and J. Sun, *Materials Science in Semiconductor Processing*, 2021, DOI: 10.1016/j.mssp.2021.105841, 105841.